Electrochemical Desorption of Thiolates and Sulfur from Nanoparticle and Planar Platinum Surfaces

María Alejandra Floridia Addato,[†] Aldo Rubert,[†] Guillermo Benítez,[†] Eugenia Zelaya,[‡] Gema Cabello,[§] Angel Cuesta,[§] Jorge E. Thomas,[†] Arnaldo Visintín,[†] Roberto C. Salvarezza,[†] and Mariano H. Fonticelli*,[†]

[†]The Research Institute of Theoretical and Applied Physical Chemistry (INIFTA), National University of La Plata - CONICET, Sucursal 4 Casilla de Correo 16, 1900 La Plata, Argentina

[‡]Bariloche Atomic Center, National Atomic Energy Commission - CONICET, Av. Bustillo 9500, 8400 S. C. de Bariloche, Río Negro, Argentina

[§]Institute of Physical Chemistry "ROCASOLANO", CSIC, C. Serrano 119, E-28006 Madrid, Spain

Ⓢ Supporting Information

ABSTRACT: Thiolate-protected platinum nanoparticles have become promising for applications in heterogeneous catalysis and the fabrication of new materials for hydrogen storage. Once nanoparticles have been synthesized and conveniently grafted onto a particular support, thiol removal might be required before its use. Here, thiolate and sulfur electrodesorption from nanoparticle and planar platinum surfaces are comparatively studied by combining ex-situ X-ray photoelectron spectroscopy (XPS) and electrochemical techniques. We show that alkanethiolates and sulfur adsorbed on Pt surfaces are more stable against reductive desorption than these species on Au substrates. Furthermore, for short-chain thiol-capped platinum nanoparticles we observe complete removal of sulfur-containing species. Hence, these results make this procedure suitable for its use in electrocatalysis. As an example, we demonstrate that 2 nm thiomalic acid-protected platinum nanoparticles markedly improve the performance of a hydrogen storage alloy material, with no additional steps in the preparation of the electrodes.
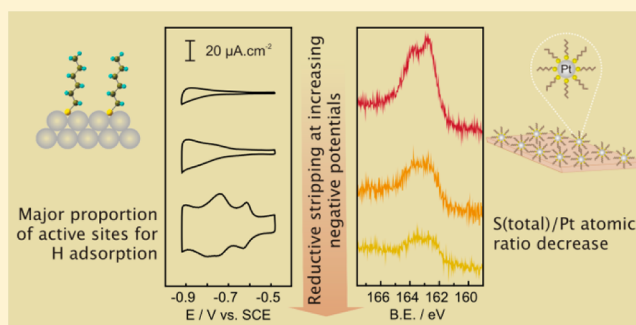
1. INTRODUCTION

Metallic nanoparticles have attracted much interest in chemistry and physics because they possess properties quite distinct from normal bulk materials.[1] Particularly, the synthesis and characterization of Pt-based nanoparticles have demonstrated to be very dynamic fields of research due to their wide range of applications.[2,3] In fact, platinum nanoparticles (PtNPs) can be used in homogeneous and heterogeneous catalysis,[4,5] in electrocatalysis,[6,7] and as sensor and biosensor platforms.[8] They can also improve the ability of new materials for hydrogen storage devices[9,10] and constitute one of the most promising materials for the next generation of ultrahigh-density magnetic storage media.[11] Therefore, there has been a special effort to design new methodologies for the preparation of PtNPs with well-defined chemical and physical properties. In this regard, the possibility of tuning the composition, morphology, and electronic properties of these materials by controlling the preparation conditions is particularly interesting.

Colloidal synthesis of metallic nanoparticles presents some advantages over the usual physical methods for the preparation of nanomaterials with controlled size and shape.[1] Three main methods based on colloid chemistry are used: (i) chemical reduction of metal salt precursors, (ii) electrochemical

synthesis, and (iii) controlled decomposition of organometallic compounds and metal—surfactant complexes.[12] In most cases this type of synthesis involves the use of organic capping agents, such as thiols or other types of surfactants, whose role is protecting and stabilizing the nanoparticles. However, the presence of an organic capping agent can have detrimental effects for some applications such as catalysis because active sites at the surface can be blocked or the electronic properties of the nanoparticles can be modified.[13,14] This is particularly important for thiol-capped PtNPs since thiolates can often hinder catalytic activity due to their strong coordination.[15] Furthermore, it is well-known that S, a possible undesired reaction byproduct of thiol self-assembly on Pt,[16] is considered as poison in heterogeneous catalysis. Although there are some examples of positive effects of adsorbed S[17] and thiolates[18] on the catalytic activity or selectivity of platinum group metals, in most cases they act as inhibitors. Therefore, the removal of these species from the metal surface needs to be considered. Several methods to overcome this issue have been reported.

For instance, thermal desorption can be an alternative for this purpose, but it could induce nanoparticle sintering and aggregation.[19] Thiols can also be oxidatively stripped from the metal surface, using either chemical agents (such as piranha solutions), ultraviolet irradiation, or electrochemical treatments. Although these strategies are often satisfactory, may, however, have undesired effects on the surface integrity and composition.[19−21] Thiolate stripping by treatment with reducing agents, such as $NaBH_4$, has also been proposed as a method for removing thiols.[22] As surface damage is not expected through the reductive desorption methods, they appear to be more suitable to perform a controlled cleaning of the metallic surfaces. In connection with it, S was reductively desorbed from TiO_2-supported Au and Pt nanoparticles in water at room temperature by UV-light irradiation.[23−25]

In this work we have made a comparative study of thiolate and S desorption from planar and nanoparticle Pt surfaces, using X-ray photoelectron spectroscopy (XPS) and electrochemical techniques to provide information on the chemical state of the metal surface and the adsorbates. Additionally, infrared spectroscopy (IR) was used to investigate the presence and order of the thiol hydrocarbon chains. Our results show that thiols and S can be desorbed from the different Pt surfaces by a reductive stripping procedure. The thiolates begin to be desorbed in the hydrogen adsorption region. However, they massively leave the Pt surface at potentials well beyond the onset of the hydrogen evolution reaction (HER). We also demonstrate that the activated PtNPs efficiently improve the performance of hydrogen storage alloy materials. The methodology proposed in this work may give rise to the use of thiol-capped PtNPs in many applications of material science, as these capping agents can be easily removed by a one-step procedure, leading to Pt sites which show high surface activity.

2. EXPERIMENTAL METHODS

Bulk Pt was modified following already reported protocols and materials.[16] More detailed information regarding the preparation of the Pt substrates can be found in the Supporting Information.

Electrochemical data have been taken by two main set of measurements involving different conditions.

The electrodesorption of thiols from Pt surfaces have been studied in a standard three-electrode electrochemical cell by means of an operational amplifier potenciostat (TEQ-Argentina). A saturated calomel electrode (SCE) and a large-area platinum foil were used as reference and counter electrode, respectively. All potentials in the text are referred to the SCE scale, unless otherwise stated. This set of measurements was performed in a 0.1 M NaOH aqueous solution as the base electrolyte, prepared from solid NaOH (analytical grade from Baker). In all cases the solutions were prepared with Milli-Q water and degassed with purified nitrogen prior to the experiments. All measurements were performed at room temperature.

Electrochemical measurements with the hydrogen storage electrodes were made in a three-compartment cell with the corresponding working electrode (metal hydride electrode), counter electrode (sintered NiOOH), and reference electrode (Hg/HgO electrode). The electrolyte, 6 M KOH solution, was prepared from reagent-grade KOH and deionized water. The experiments were carried out at 298 K. The discharge capacity was determined as a function of the charge−discharge cycling number. In order to perform this operation, a fixed cathodic

current of 10 mA was applied for 9000 s to ensure the full charge of the electrode. The discharge was conducted at a constant anodic current of 5 mA until the cutoff potential (−0.6 V vs Hg/HgO). Before the electrochemical impedance spectroscopy (EIS) measurements, the electrodes were charge−discharge-cycled at a constant current for 25 cycles. After cycling, the electrodes were discharged to a state of charge of 50% and left at open circuit potential (E_o) for 15 min. The EIS spectra were recorded, at E_o, in the 10 kHz−1 mHz frequency range, with a 5 mV amplitude.

The samples were characterized by XPS using a Mg Kα source (XR50, Specs GmbH) and a hemispherical electron energy analyzer (PHOIBOS 100, Specs GmbH). XPS was also performed at the SGM beamline of the Laboratório Nacional de Luz Síncrotron (LNLS), Campinas, Brazil, with a hemispherical electron energy analyzer (PHOIBOS 150, Specs GmbH). The energy of the incident photons was set to 250 eV.

Surface-enhanced infrared absorption spectroscopy in the attenuated total reflection mode (ATR-SEIRA) was performed in the Kretschmann configuration with a Nicolet 6700 FTIR spectrometer equipped with a liquid nitrogen-cooled mercury−cadmium−telluride (MCT) detector, using p-polarized light. Spectra are the result of adding 10 interferograms and were recorded with a 4 cm^{-1} resolution. Additional experimental details can be found in the Supporting Information.

Dodecanethiolate- and thiomalic acid-protected PtNPs were synthesized by the methods reported by Eklund et al.[15] and by Chen and Kimura,[26] respectively. Details on the synthesis of the nanoparticles are given in the Supporting Information.

Transmission electron microscopy (TEM) imaging of PtNPs was performed using a FEI CM200 UT microscope, operating at 200 kV. The images were taken with the nanoparticles supported on 300 mesh ultrathin carbon film on holey carbon support gold grids. The size distribution of nanoparticles was performed using ImageJ software[27] by measuring 500 nanoparticles from bright-field images. A log-normal distribution function was fitted to the histogram obtained, according to ref 28. The low-magnification micrographs were taken in overfocus in order to improve the contrast with the carbon layer.

Scanning tunneling microscopy (STM) images were obtained in air with commercial Pt−Ir tips using a Nanoscope IIIa microscope from Veeco Instruments (Santa Barbara, CA). Typical tunneling currents and bias voltages for PtNPs imaging were 100 pA and 1000 mV, respectively.

The metal hydride electrodes were made by mixing 75 mg of the lanthanide mischmetal-based (Lm) alloy, hereinafter referred as AB_5-type alloy, with nominal composition $LmNi_{4.1}Co_{0.4}Mn_{0.4}Al_{0.5}$[29] and 75 mg of Vulcan XC72R teflonized with 33 wt % polytetrafluoroethylene (PTFE). The mixture was then pressed onto nickel mesh under a pressure of 2000 kg cm^{-2} inside a 1 cm^2 section cylindrical die.

To study the effect of PtNPs on this system, a suspension of the thiomalic acid-capped nanoparticles in ethanol were added to the AB_5-type alloy, dried, and mixed whit the teflonized Vulcan. The amount of PtNPs added was equivalent to 1 wt %.

3. RESULTS AND DISCUSSION

3.1. XPS and Infrared Spectroscopy Characterization of the Hexanethiol and Dodecanethiol Self-Assembled Monolayers on Polycrystalline Pt Surfaces. Self-assembled monolayers (SAMs) of thiols on Pt have been characterized by using different techniques.[30−33] There exists a general agreement that these SAMs exhibit a more complex surface

chemistry than those formed on Au. In fact, on the platinum group metals, adsorbed sulfur can be formed from C–S bond scission due to their catalytic activity.[16,34,35]

In a previous work, XPS and electrochemical data indicated that dodecanethiol (DT) SAMs on Pt surfaces exhibit barrier properties similar to those on Au, while hexanethiol (HT) forms more defective SAMs.[16] The XPS S 2p regions of HT and DT on Pt were successfully fitted by a set of two doublets at 162.3 eV (C2) and 163.4 eV (C3). The C2 component has been assigned to sulfur and/or thiolates, since both species lie at the same binding energy (BE) value for Pt.[36] On the other hand, the C3 component has been assigned to "unbound" alkanethiol derived species such as alkyl disulfides,[37] dialkyl sulfides,[38] and dimerized thiolate species.[39,40] Here, in order to gain insight into the nature and abundance of the sulfur species, more accurate X-ray photoelectron spectra and a higher surface sensitivity have been achieved with synchrotron radiation. For HT-covered Pt surfaces (Figure 1a) the two main doublets C2
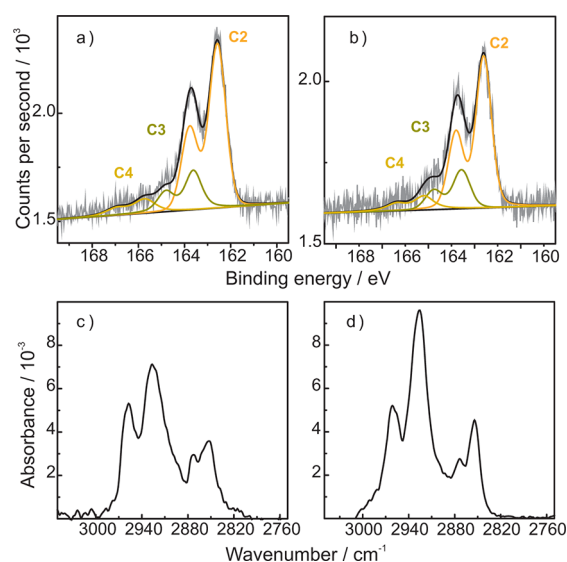
Figure 1. High-resolution S 2p XPS spectrum for (a) HT SAM and (b) DT SAM on Pt surfaces. The three components (C2 at 162.6 eV, C3 at 163.6 eV, and C4 between 165.2 and 165.8 eV) are indicated. ATR-SEIRA spectra, recorded in ambient atmosphere, of HT (c) and DT (d) adsorbed on Pt.

(162.6 eV) and C3 (163.6 eV) contribute with 70% and 20%, respectively. Interestingly, there is no contribution of sulfur species of BEs smaller than 162 eV. This is an indication that atomic sulfur has low coverage, since at intermediate or high coverages it shows a contribution at ~161 eV.[36] As mentioned above, the C2 component can have contributions from both low-coverage atomic sulfur and thiolates. However, neither the separation between the well-resolved $2p_{3/2}$ and $2p_{1/2}$ peaks, which is close to the spin–orbit splitting of 1.2 eV, nor the full width at half-maximum of the $2p_{3/2}$ peak (0.84 eV) justifies the addition of another doublet in this BE region. Therefore, low coverage atomic sulfur and thiolate could not be distinguished in the XPS spectrum of HT on Pt. The smallest doublet (C4) (S $2p_{3/2}$ component at 165.8 eV in Figure 1a) could not be observed in the conventional XPS spectra, but it is apparent in synchrotron-based measurements of thiol SAMs on Pt.[38] Finally, neither sulfates nor sulfonates (S 2p BE > 166 eV) were detected by XPS on any of the samples.

The structure and organization of these systems have also been studied by ATR-SEIRAS. Four main bands, whose assignment has been widely discussed in the literature,[30,37,41,42] can be distinguished in the C–H region, related to the IR-active alkyl modes. The most intense band, at 2925 cm^{-1}, arises from the antisymmetric methylene stretching, whereas the symmetric mode appears around 2854 cm^{-1}. The two remaining bands at 2961 and 2874 cm^{-1} are related to the antisymmetric and the symmetric methyl stretches, respectively.

The intensity of the symmetric CH$_2$ stretching mode increases (relative to the symmetric CH$_3$ stretching mode) from the HT SAM to the DT SAM, as expected from the increase in the chain length. This suggests that the integrity of the alkanethiolate is maintained upon adsorption. The lower intensities of the CH$_2$ peaks, as compared with SAMs of the same thiols on Au, have been related to an almost perpendicular orientation of the alkyl moieties on Pt.[37,43]

3.2. Desorption of Thiolate–Sulfide Adlayers from Polycrystalline Pt Surfaces. Electrochemistry provides suitable tools for the study of the desorption of alkanethiolates and S from metallic surfaces.[44] Usually, the electrodesorption of thiols from metal surfaces is studied in aqueous alkaline solutions[45,46] since thiols predominate in their anionic forms facilitating the process. Note that in these solutions the anionic species have higher solubility than the corresponding molecular forms, which predominate in neutral or acid media. For instance, studies performed on Au(111) have shown the importance of the thiol solubility on its complete removal of the surface. As claimed by the authors, the more soluble the thiol, the smaller the extent of the oxidative redeposition.[47] Therefore, the attainment of a clean surface might be expected in alkaline media, at pHs higher than the pK_a value of the thiol.

Reductive desorption curves, generally obtained by linear sweep voltammetry, have been extensively used to obtain information about stability and coverage of these species on Au and Ag.[48–50] In contrast, on Pt, Pd, or Ni, the negative potential scans reach the hydrogen evolution region before any evidence of reductive desorption peaks.[46,51] Therefore, in order to study the electrodesorption of thiolate and S, we have used voltammetric capacitance (C), hydrogen adsorption charge, and XPS data.

Capacitance data were recorded after polarizing the Pt electrodes at different negative potential limits (E_c). The values were obtained by dividing the charging current density (j) by the scan rate (v) in a potential range where no faradaic processes occur. For the clean metal, the current density is almost constant within a narrow potential range, between $E = -0.48$ and $E = -0.53$ V vs the SCE, in 0.1 M NaOH (inset Figure 2a). Although the generally accepted definition of double-layer region for platinum-group metals, i.e., a flat region appearing in cyclic voltammogram,[52] is fulfilled in this potential domain, it must be taken into account that in alkaline media H and OH adsorption overlaps in this region.[53] For simplicity, we analyze the remaining coverage, θ_C, which is obtained from the capacitance measurements[54,55] according to eq 1

$$\theta_C = [C_{clean} - C_{E_c}/(C_{clean} - C_{mono})] \tag{1}$$

where C_{E_c} and C_{clean} are the capacitance values estimated at each E_c and that measured for a clean Pt surface, respectively, and C_{mono} stands for the capacitance of the electrode with the maximum surface excess of the adsorbate. It is worth noting that the quantity θ_C does not represent a real coverage and
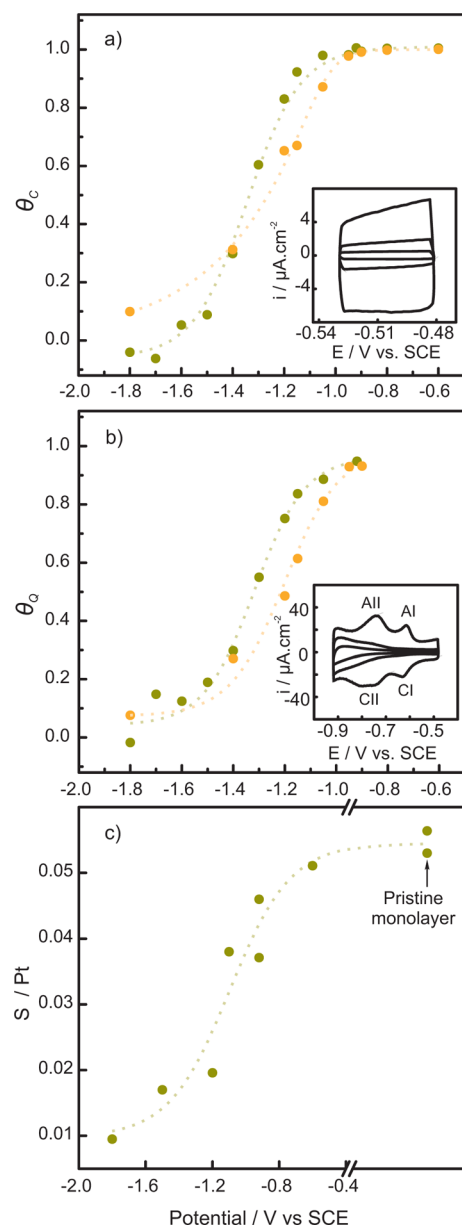
Figure 2. Effect of polarizing the HT (green) and DT (orange) SAM-covered Pt substrates at different negative potentials (E_c) in 0.1 M NaOH: (a) residual coverage obtained from interfacial capacitance; (b) proportion of Pt sites, θ_Q, still blocked. The insets in (a) and (b) show voltammograms used to estimate the capacitance and hydrogen charge density, respectively, of HT SAM-covered substrates. (c) S(total)/Pt atomic ratio obtained from the XPS spectrum of a HT SAM-covered substrate and after each applied E_c.

should not be compared with the coverage obtained from XPS data. The idea behind the use of θ_C is to find a normalizing factor.

It is clear from Figure 2a that, between −0.60 and −0.80 V, the θ_C remains constant; i.e., the Pt surface remains covered by the adsorbates. Massive desorption occurs for $E_c < -1.0$ V, as reflected by the large decrease in θ_C (Figure 2a). Finally, at $E_c < -1.6$ V, θ_C reaches values below 0.1 (close to 0 for the case of HT). This means that most of the adsorbates desorb after polarization to very negative potentials.

However, capacitance measurements do not inform about the presence or absence of adsorbed S, which can be formed

upon S−C bond breaking, because the S adlayer also exhibits large C values.[16] Thus, the availability of Pt sites for hydrogen adsorption after adsorbate removal was studied by means of cyclic voltammetry (inset in Figure 2b). The voltammogram of a clean Pt surface shows the underpotential deposition (upd) of H atoms at peaks CI (strongly adsorbed H) and CII (weakly adsorbed H), which are desorbed at peaks AI and AII, respectively. It is noticeable that the sulfur adsorbates almost completely block the formation of hydrogen adatoms. However, polarization at potentials progressively more negative produces thiolate desorption and leaves more free sites for hydrogen adsorption. The charges (Q_H) related to the H adsorption and desorption after removal of the S containing species were measured in order to compute the number of available Pt sites. The Q_H values were determined after the capacitance measurements at any E_c. The inset in Figure 2b shows cyclic voltammograms obtained after applying −0.92, −1.2, and −1.8 V on an initially modified HT electrode. The results show that the more negative E_c, the higher the hydrogen adsorption and desorption current densities due to adsorbate removal from the Pt surface. For the sake of comparison, we define a residual coverage, θ_Q, with the aim of normalizing the charges computed in each case

$$\theta_Q = 1 - (Q_{H\,E_c}/Q_{H\,\text{clean}}) \tag{2}$$

where $Q_{H\,E_c}$ and $Q_{H\,\text{clean}}$ are the hydrogen adsorption charges at each E_c and that measured for a clean Pt surface, respectively. The θ_Q vs E_c plot (Figure 2b), which reflects the proportion of Pt sites still blocked, also shows that the adsorbed species start to leave the Pt surface for $E_c < -0.9$ V and that at $E_c < -1.6$ V the number of free Pt sites is similar to that measured on the clean surface.

The conclusions reached from the electrochemical quantities shown in Figure 2a,b were confirmed by the XPS measurements for pristine monolayers and after polarizing the HT-covered Pt electrode at different E_c values (Figure 2c). We note that the S(total)/Pt ratio vs E_c plot follows the same trend as that observed for the total amount of adsorbates vs E_c determined by the electrochemical measurements (Figure 2a,b).

It is interesting to compare the desorption of HT SAMs from Pt and Au surfaces in the same electrolyte solution. It is well established that in 0.1 M NaOH HT starts to desorb from Au surfaces at ~−0.9 V, the peak potential (E_p) for this process being located at −0.96 V (i.e., about 50% of the HT molecules are desorbed at −0.96 V). In contrast, for the HT SAM on Pt, removal of 50% of the adsorbate is achieved between −1.2 and −1.4 V (Figure 2). Our results are in qualitative disagreement with those reported by Williams et al. According to their study, it should be easier to desorb SAMs of alkanethiols on Pt than from Au.[51] The redox probe employed by these authors is suitable for detecting the onset of alkanethiol desorption, but not to decide whether the electrode can be efficiently cleaned (Figure S2). Indeed, if partial desorption occurs, the electrode would behave as a microelectrode ensemble, which may show the same voltammetric profile than the clean surface.[56−58]

The greater stability of thiolates on Pt in comparison with Au can be related to their larger binding energy (ε_b) on Pt. For instance, DFT calculations for methylthiolate on Pt(111) yield an ε_b between −2.5 and −2.8 eV,[16,59] while on Au(111) ε_b lies between −1.8 and −2.6 eV, depending on the surface model used for the calculations.[60] Also, it can be explained in terms of

the differences in bonding character for S−Pt and S−Au. Thiolate adsorption on Au has a considerable contribution from the s-states of the metal. For Pd and Pt, the strong covalent interaction between adsorbate and substrate involves mostly the sulfur p-states and the metal d-band, leading to a weaker C−S bond.[59] In particular, DFT calculations have shown that the C−S bond breaking in thiol SAMs on Pd is a consequence of the d-band location close to the Fermi level.[61]

It is well-known that chemisorbed thiolates can be reductively desorbed from metal surfaces (M) in alkaline solutions through the reaction

$$RS-M + e^- = RS^- + M \qquad (3)$$

where RS^- represents the thiolates. Alternatively, chemical desorption by atomic hydrogen has been used to remove the thiols from the Au(111) surface.[62,63] In that case, atomic hydrogen was introduced into the vacuum chamber, and it led to the complete removal of thiols from the surface according to the reaction

$$RS-M + H = RSH + M \qquad (4)$$

On clean Pt electrodes, adsorbed atomic H is produced in situ at $E_c < -0.6$ V (inset Figure 2b) by the Volmer reaction:

$$H_2O + e^- = H_{ad} + OH^- \qquad (5)$$

Reaction 5 provides the atomic hydrogen needed for reaction 4. Therefore, thiol desorption from Pt surfaces could take place by reactions 3 and/or 4. The fact that the thiol desorption curves ($E_c < -0.9$ V) do not follow the H adsorption profile on clean Pt ($E_c < -0.6$ V) can be easily explained considering the difficulty to transport water to the Pt surface through the hydrophobic SAM, which introduces an important overvoltage for reaction 5. In addition, since sulfur-containing species are more strongly adsorbed than those species coming from the solution, the replacement of adsorbates is not expected to follow the same behavior.

The above-discussed data apply to the short-chain HT, which is partially soluble as hexanethiolate in 0.1 M NaOH. In Figure 2a,b we have also included desorption data for the longer and more insoluble DT. We note that SAM desorption becomes also evident at $E_c < -0.9$ V, in the same potential range as for HT SAMs. It could be expected that complete removal of DT cannot be achieved, since micelle formation could take place on the Pt surface.[60] However, on Pt surfaces a reasonable cleanness is also achieved for DT (Figure 2), probably due to the very high negative potentials involved and the simultaneous HER that induces convective transport to the solution.

We have also tested the electrochemical cleaning procedure for SAMs of short, water-soluble thiols, using thiomalic acid (TMA) as a probe molecule. The more defective nature of the TMA SAM is evident from the fact that at −0.9 V there is ≈20% of Pt active sites for hydrogen adsorption (Figure S3), while this number is only 10% for HT and DT SAMs (Figure 2). In the case of TMA, most of the thiol-derived species at the interface have been desorbed at −1.6 V.

As discussed above, traces of S can also be found on Pt surfaces modified with thiol SAMs. For this reason, we also studied the desorption of sulfide from sulfide-modified Pt surfaces (Figure S4). Sulfide desorption starts in the same potential range previously observed for thiol modified surfaces. After applying increasing negative potentials the hydrogen adsorption and desorption charge densities reach ≈95% of the value observed for the clean surface. This means that an almost

complete removal of the S layer is also possible by the reductive stripping procedure.

As a summary of this section, the stability potential range for the adsorbate is the same for the different sulfur species considered in the current study. The desorption processes start concomitantly with H adsorption, and the massive desorption occurs in the potential range −1.0 V > E_c > −1.6 V. Thus, the electrochemical desorption is a suitable tool to remove thiols and sulfur from bulk Pt.

3.3. Desorption from Nanoparticle Pt Surfaces. We can now analyze the possibility of cleaning thiolate-capped PtNPs by the electrochemical reductive stripping procedure described for planar surfaces. This deserves special attention because there exist some important differences between planar polycrystalline surfaces and nanoparticles. First, it has been reported that reductive desorption of thiolates from Au nanoparticles occurs at more negative potentials than from planar Au surfaces.[64] This is not surprising because thiolates are strongly chemisorbed on defective (low coordinated) metallic sites.[65] As suggested above, in the case of polycrystalline Pt, H adsorption could play an important role in the desorption of thiolate SAMs (reactions 4 and 5). However, it has been proposed that the strength of H adsorption on Pt decreases along with particle size, whereas the energy of adsorption of anions increases with decreasing particle size.[66] As a consequence, the reductive stripping of thiolate from PtNPs must be studied in detail.

In our study we have used thiolate-capped PtNPs supported on highly oriented pyrolitic graphite (HOPG) because carbon is usually employed as a substrate for Pt nano/micro particle dispersion in heterogeneous catalysis. Besides, the HOPG surface is chemically inert, thus avoiding a strong interaction of the substrate with the desorbed thiols.[67] Figure 3a shows TEM images of DT-covered PtNPs. The size distribution function indicates that they are monodisperse and extremely small with 1.8 ± 0.6 nm in average size (Figure 3b).

XPS data for these DT-capped PtNPs supported on HOPG recorded before and after polarization at $E_c = -1.6$ and −1.8 V are shown in Figure 3c,d. After the polarization at these negative potentials, the intensity of the Pt 4f signal (Figure 3d) slightly increases and shifts toward lower binding energies, while the intensity of the S 2p signal (Figure 3c) decreases. This decrease of the S/Pt atomic ratio can be explained by the progressive desorption of S-containing species from the Pt surface. However, the amount of S-containing species remaining at −1.8 V is ≈30% of the initial value. Thus, the electrochemical removal of DT from PtNPs is less efficient than in planar surfaces, where this quantity is smaller than 15% of the initial value. In addition to the low solubility of DT, this might be related to the stronger adsorption of thiolates on nanoparticles, as mentioned above.

In contrast, TMA-capped PtNPs of a similar size (Figure 4) are easily cleaned by the electrochemical procedure as depicted in the XPS data in Figure 5a,b.

In this case, we observe a clear shift of the Pt 4f signal to lower BE values (Figure 5b) and, more important, the complete absence of the S 2p signal after the electrochemical cleaning procedure (Figure 5a); i.e., S-containing species have been completely removed from the Pt surface. The efficiency of this procedure is also reflected in the cyclic voltammograms recorded in the hydrogen adsorption region before and after the electrochemical treatment of the TMA-covered PtNPs (Figure 5d). As can be observed, after polarizing the Au-
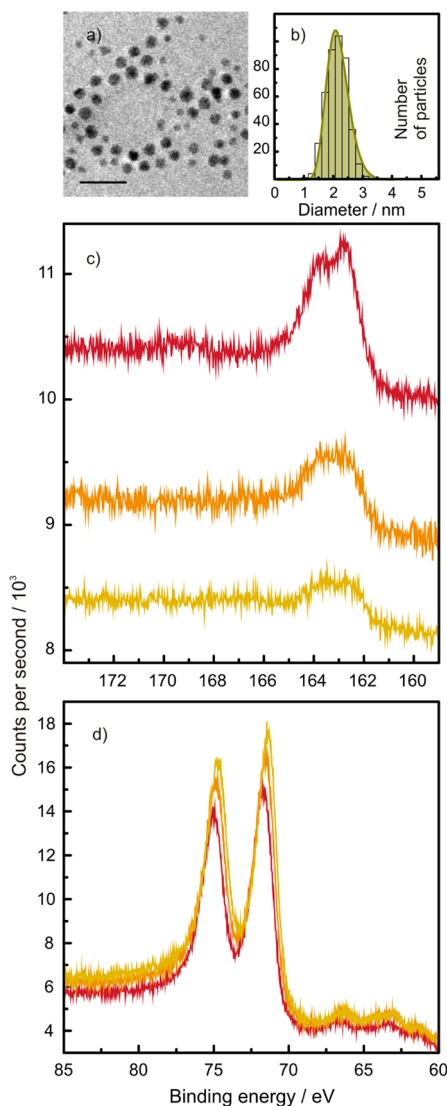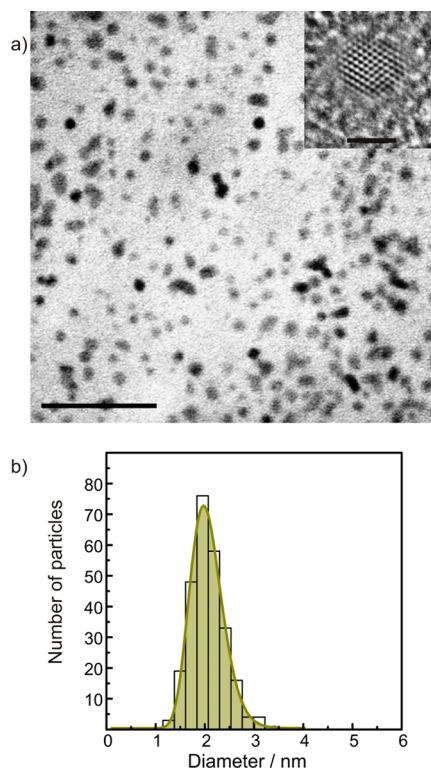
Figure 3. (a) Bright-field image of the DT-capped PtNPs (scale bar 10 nm) and (b) the corresponding size distribution histogram with its log-normal fit. (c, d) XPS spectra of the DT-capped PtNPs before (deep red) and after reductive stripping of the adlayer at −1.6 V (orange) and −1.8 V (yellow): (c) S 2p region; (d) Pt 4f region.


Figure 4. (a) Bright-field image of the TMA-capped PtNPs (scale bar 20 nm) and (b) the corresponding size distribution histogram with its log-normal fit. The inset in (a) shows a high-resolution image of one nanoparticle (scale bar 2 nm).

supported PtNPs at E_c = −1.8 V, the H adsorption current peaks are recovered on the Pt surface. In addition, STM images of the NPs supported on the HOPG surface (Figure 5c) demonstrate that no significant sintering takes place during the polarization at these negative potential values. At first glance, the PtNPs seem to be greater than the TMA-capped ones, imaged by TEM. However, we consider that this is due to tip−sample convolution which limits the resolution. As a consequence, very small adjacent nanoparticles appear as just one feature.[68]

As discussed for planar Pt surfaces, the solubility of the thiols might be important to attain clean surfaces. Indeed, aside from the fact that thiols adsorb more strongly on nanoparticle surfaces than on bulk Pt, the high solubility of the thiomalate anions on alkaline solutions might be beneficial for the desorption process.

3.4. Pt Nanoparticles as Additives in Metal Hydride Electrodes. PtNPs have been extensively used as active surfaces in multicomponent materials. Their ability to catalyze,

among other processes, the electrochemical hydrogen reaction offers the possibility of designing composite materials for hydrogen storage. In fact, metal hydride alloys, commonly found in alkaline batteries, dosed with different electrocatalytic metals have been widely used for this purpose. The addition of these electrocatalysts accelerates the activation of the metal alloy, which is the rate-determining step in the absorption/desorption process. The thiol-capped PtNPs studied in this work are easily adaptable to these electrodes because their stability in alkaline medium has been previously assessed. Furthermore, the electrochemical treatment required prior to their use promotes the removal of the thiol, leaving a cleaner surface.

In order to test the possible use of thiol-capped PtNPs to improve the performance of hydrogen storage materials, they were added to metal hydride electrodes. Both kinds of electrodes, the mischmetal-based alloy and that material modified by 1 wt % of PtNPs, were exhaustively characterized by electrochemical techniques (Figures S5−S11).

According to the results regarding the reductive stripping cleaning procedure (see above), the onset of TMA removal from PtNPs should be exceeded during the cathodic charge of the metal hydride electrodes. As sulfur species desorb from PtNPs, Pt sites available for H adsorption are formed. Thus, the Volmer reaction leads to H adatoms which can spill over from the surface of the alloy particles and are absorbed into the lattice (Scheme 1). Alternatively, the adatoms can form molecular hydrogen that will leave the interface.

Figure 6a shows that 1 wt % of PtNPs addition to a mischmetal alloy improves the capacity of hydrogen storage of the electrodes in ~10%. This improvement could be explained
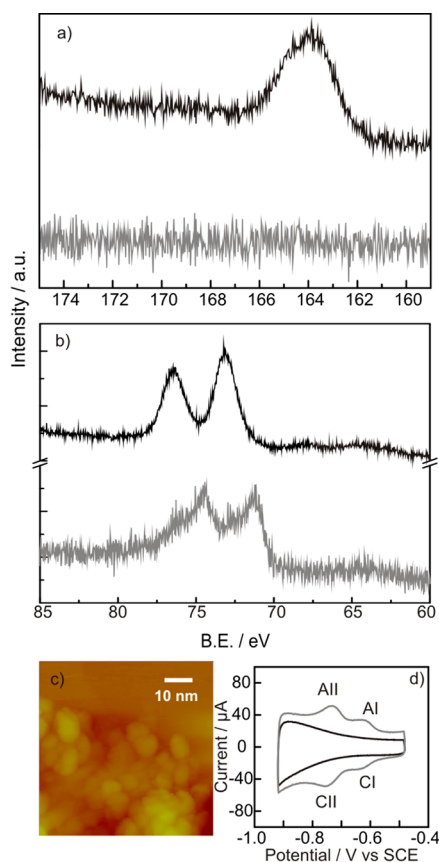
Figure 5. (a) S 2p and (b) Pt 4f regions of the XPS spectrum of TMA-covered PtNPs before (upper trace) and after (bottom trace) reductive stripping at −1.8 V. (c) STM image of the clean PtNPs supported on HOPG. (d) Cyclic voltammograms of the PtNPs supported on Au in 0.1 M NaOH, recorded after reductive stripping at $E_c = -0.92$ V (black trace) and at $E_c = -1.8$ V (gray trace). Scan rate = 100 mV s^{-1}.

Scheme 1. Representation of the Cleaning/Activation Processes[a]
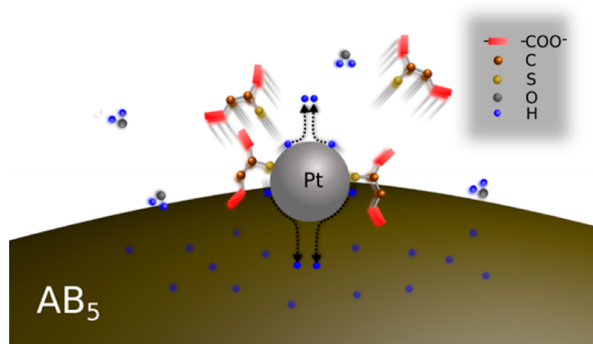
[a]Sulfur species desorb from the surface of PtNPs; hydrogen molecules dissociate into hydrogen atoms on the surface of the PtNPs; hydrogen atoms spill over from the Pt surface and are absorbed into the alloy lattice. Also, hydrogen adatoms that form molecular hydrogen are represented.

taking into account that the PtNPs enhance the kinetics of the Volmer reaction (5), which increases the amount of hydrogen available on the alloy surface for the hydrogen absorption reaction. Indeed, the exchange current density for the HER on the surface of PtNPs in alkaline media is almost 3 times higher than on AB$_5$-type alloy particles.[69,70] Additionally, the active
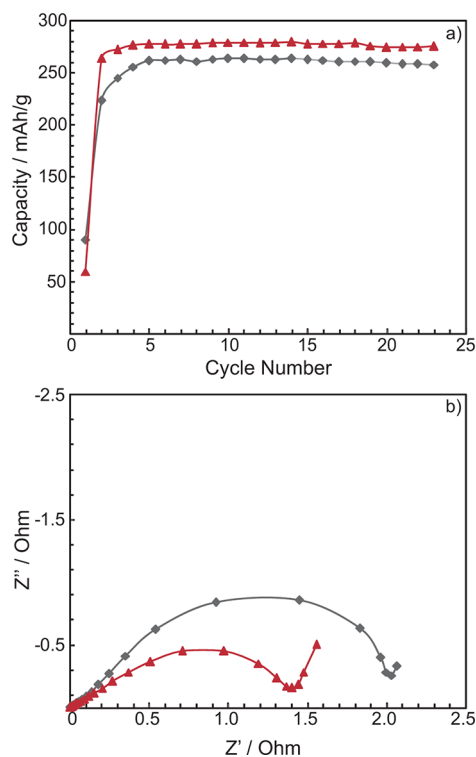
Figure 6. (a) Discharge capacities of the hydrogen storage electrodes versus cycling number, conducted at 5 mA after charging the electrode at 10 mA during 9000 s in 6 M KOH and (b) EIS measurements represented on Nyquist diagrams carried out throughout the charge–discharge cycling. Gray diamonds and red triangles correspond to the mischmetal alloy and the alloy containing 1 wt % of TMA-capped PtNPs, respectively.

area increases significantly when 1% of PtNPs (diameter ≈ 1.8 nm) is added to AB$_5$ alloy (diameter ≈ 10 μm).[71] It is known that the limitations to achieve increased charge densities and the appearance of high charge overpotentials for the charging of metal hydride electrodes arise from surface oxide films, which are formed during metal alloy exposure to air.[72] Thus, after thiolate desorption from the Pt sites, which occurs during the activation of the alloys, the surface oxide reduction is promoted either by the hydrogen atoms or by the produced molecular hydrogen.

More important, the EIS results demonstrate the influence of the PtNPs for improving the electrode kinetics. In fact, the Nyquist diagrams (Figure 6b) show that PtNPs markedly decrease the charge transfer resistance. After fitting the EIS data to a physicochemical model proposed previously,[73] it was possible to determinate that the charge transfer resistance diminishes from 1.958 to 1.156 Ω upon the addition of the PtNPs. A similar upturn in the behavior of AB$_5$ alloys has been reported,[72] but upon addition of a higher amount of Pt (Pt powder from 5 to 20 wt %). In the present study, very small PtNPs were used, which present a high fraction of the atoms on their surface. Thus, an improved performance of the alloy electrodes was observed at low Pt loadings (∼1 wt %) due to the high Pt dispersion on the alloy surface.

There are additional points that might be commented with regards to the technological viability of the present desorption method. First, there is a high exploitation of the Pt, which is an expensive metal. For instance, consider that for fcc cubooctahedral perfect Pt crystallites of 1.8 nm 60% of the

metal atoms are on the surface.[74] The narrow size distribution of these particles and the possibility of tuning the mean size of the product through changes of the synthesis parameters represent distinguishing features with regards to applications. It is also worth noting that the possible byproducts of the nanoparticles' synthesis, that might contain Pt species, and the particles of bigger sizes, could be recovered. Second, other methods to remove the capping agents are not suitable for the kind of material used in this study. Indeed, the mischmetal alloys cannot be processed at high temperatures or exposed to the extremely oxidant conditions necessary to remove thiols.[19] Similarly, the mild conditions used to remove weakly adsorbed species[75] would not be useful to desorb the strongly bound thiolates. Third, neither inclusion of the PtNPs nor desorption of the capping-species implied additional steps in the preparation of the electrodes.

4. CONCLUSION

Self-assembled monolayers of thiols on Pt nanoparticles and planar surfaces have been characterized, and its stability against electrochemical polarization at very negative potentials was investigated. Thiolates and sulfur were desorbed from platinum in potential regions that favor cathodic processes, thus reducing the risk of producing deep changes on the structure of the surfaces. In contrast to previous findings for alkanethiolates on Pt in methanolic solutions,[51] complete thiolate desorption in aqueous 0.1 M NaOH takes place at potentials more negative than those observed for self-assembled monolayers of short thiols on Au. Furthermore, it was demonstrated that thiol-modified Pt surfaces can be efficiently cleaned by means of reductive stripping in the hydrogen evolution region. Moreover, it was found that the cleaning efficiency depends on the solubility of the thiols in the alkaline aqueous media. For instance, water-soluble thiols can be completely removed from the surface of Pt nanoparticles. On the contrary, the method fails for dodecanethiol because the desorbed products remain at the metal/water interface.

Regarding the possible technological application of Pt nanoparticles protected by thiolates, it is worth noting that these materials were prepared and manipulated as stable products. The particles prepared in the presence of the water-soluble thiomalic acid were supported on carbon substrates, and the capping agent was removed by simple and fast electrochemical cleaning. We have also demonstrated that these Pt nanoparticles improve the performance of hydrogen storage alloys. The low Pt loading required and the fact that no additional operations were needed to prepare the Pt-modified alloys make the methodology presented here suitable for its application in hydrogen storage materials.

ASSOCIATED CONTENT

Ⓢ Supporting Information
More detailed information about the experiments performed in this work. This material is available free of charge via the Internet at http://pubs.acs.org.

AUTHOR INFORMATION

Corresponding Author
*Fax +54 221 425 4642; phone +54 221 425 7430; e-mail mfonti@inifta.unlp.edu.ar.

Notes
The authors declare no competing financial interest.

ACKNOWLEDGMENTS

REFERENCES

(1) Talapin, D. V.; Lee, J.-S.; Kovalenko, M. V.; Shevchenko, E. V. Chem. Rev. 2009, 110, 389−458.
(2) Le Guével, X.; Trouillet, V.; Spies, C.; Jung, G.; Schneider, M. J. Phys. Chem. C 2012, 116, 6047−6051.
(3) Peng, Z.; Yang, H. Nano Today 2009, 4, 143−164.
(4) Narayanan, R.; El-Sayed, M. A. Nano Lett. 2004, 4, 1343−1348.
(5) Narayanan, R.; El-Sayed, M. A. J. Phys. Chem. B 2005, 109, 12663−12676.
(6) Antolini, E. Appl. Catal., B 2009, 88, 1−24.
(7) Hu, J.; Lu, X.; Foord, J. S. Electrochem. Commun. 2010, 12, 676−679.
(8) Hrapovic, S.; Liu, Y.; Male, K. B.; Luong, J. H. T. Anal. Chem. 2003, 76, 1083−1088.
(9) Li, Y.; Yang, R. T.; Liu, C.; Wang, Z. Ind. Eng. Chem. Res. 2007, 46, 8277−8281.
(10) Bhowmick, R.; Rajasekaran, S.; Friebel, D.; Beasley, C.; Jiao, L.; Ogasawara, H.; Dai, H.; Clemens, B.; Nilsson, A. J. Am. Chem. Soc. 2011, 133, 5580−5586.
(11) Sun, S. Adv. Mater. 2006, 18, 393−403.
(12) Jia, C.-J.; Schuth, F. Phys. Chem. Chem. Phys. 2011, 13, 2457−2487.
(13) Li, D.; Wang, C.; Tripkovic, D.; Sun, S.; Markovic, N. M.; Stamenkovic, V. R. ACS Catal. 2012, 2, 1358−1362.
(14) Biswas, M.; Dinda, E.; Rashid, M. H.; Mandal, T. K. J. Colloid Interface Sci. 2012, 368, 77−85.
(15) Eklund, S. E.; Cliffel, D. E. Langmuir 2004, 20, 6012−6018.
(16) Floridia Addato, M. A.; Rubert, A. A.; Benítez, G. A.; Fonticelli, M. H.; Carrasco, J.; Carro, P.; Salvarezza, R. C. J. Phys. Chem. C 2011, 115, 17788−17798.
(17) Park, I.-S.; Xu, B.; Atienza, D. O.; Hofstead-Duffy, A. M.; Allison, T. C.; Tong, Y. J. ChemPhysChem 2011, 12, 747−752.
(18) Marshall, S. T.; O'Brien, M.; Oetter, B.; Corpuz, A.; Richards, R. M.; Schwartz, D. K.; Medlin, J. W. Nat. Mater. 2010, 9, 853−858.
(19) Menard, L. D.; Xu, F.; Nuzzo, R. G.; Yang, J. C. J. Catal. 2006, 243, 64−73.
(20) Mirsaleh-Kohan, N.; Bass, A. D.; Sanche, L. Langmuir 2009, 26, 6508−6514.
(21) Price, S. W. T.; Speed, J. D.; Kannan, P.; Russell, A. E. J. Am. Chem. Soc. 2012, 133, 19448−19458.
(22) Yuan, M.; Zhan, S.; Zhou, X.; Liu, Y.; Feng, L.; Lin, Y.; Zhang, Z.; Hu, J. Langmuir 2008, 24, 8707−8710.
(23) Tada, H.; Soejima, T.; Ito, S.; Kobayashi, H. J. Am. Chem. Soc. 2004, 126, 15952−15953.
(24) Kiyonaga, T.; Kawahara, T.; Tada, H. Electrochem. Solid-State Lett. 2006, 9, E9−E12.
(25) Miyazaki, S.; Kiyonaga, T.; Kawahara, T.; Tada, H. Chem. Lett. 2007, 36, 1214−1215.
(26) Chen, S.; Kimura, K. J. Phys. Chem. B 2001, 105, 5397−5403.
(27) Abramoff, M. D.; Magelhaes, P. J.; Ram, S. J. Biophotonics Int. 2004, 11, 36−42.
(28) Granqvist, C. G. J. Appl. Phys. 1976, 47, 2200.
(29) Thomas, J. E.; Humana, R. M.; Zubizarreta, L.; Arenillas, A.; Menéndez, J. A.; Corso, H. L.; Visintin, A. Energy Fuels 2010, 24, 3302−3306.

7596

dx.doi.org/10.1021/jp311938u | J. Phys. Chem. C 2013, 117, 7589−7597

(30) Hines, M. A.; Todd, J. A.; Guyot-Sionnest, P. *Langmuir* **1995**, *11*, 493−497.

(31) Laiho, T.; Leiro, J. A. *Surf. Interface Anal.* **2008**, *40*, 51−59.

(32) Yang, Y.-C.; Yen, Y.-P.; Ou Yang, L.-Y.; Yau, S.-L.; Itaya, K. *Langmuir* **2004**, *20*, 10030−10037.

(33) Lee, S.; Park, J.; Ragan, R.; Kim, S.; Lee, Z.; Lim, D. K.; Ohlberg, D. A. A.; Williams, R. S. *J. Am. Chem. Soc.* **2006**, *128*, 5745−5750.

(34) Love, J. C.; Wolfe, D. B.; Haasch, R.; Chabinyc, M. L.; Paul, K. E.; Whitesides, G. M.; Nuzzo, R. G. *J. Am. Chem. Soc.* **2003**, *125*, 2597−2609.

(35) Corthey, G.; Rubert, A. A.; Picone, A. L.; Casillas, G.; Giovanetti, L. J.; Ramallo-Lopez, J. M.; Zelaya, E.; Benitez, G. A.; Requejo, F. G.; Jose-Yacaman, M.; Salvarezza, R. C.; Fonticelli, M. H. *J. Phys. Chem. C* **2012**, *116*, 9830−9837.

(36) Rodriguez, J. A.; Kuhn, M.; Hrbek, J. *Chem. Phys. Lett.* **1996**, *251*, 13−19.

(37) Petrovykh, D. Y.; Kimura-Suda, H.; Opdahl, A.; Richter, L. J.; Tarlov, M. J.; Whitman, L. J. *Langmuir* **2006**, *22*, 2578−2587.

(38) Laiho, T.; Lukkari, J.; Meretoja, M.; Laajalehto, K.; Kankare, J.; Leiro, J. A. *Surf. Sci.* **2005**, *584*, 83−89.

(39) Alonso, C.; Pascual, M. J.; Salomón, A. B.; Abruña, H. D.; Gutierrez, A.; López, M. F.; García-Alonso, M. M. C.; Escudero, M. L. *J. Electroanal. Chem.* **1997**, *435*, 241−254.

(40) Gutiérrez, A.; Alonso, C.; López, M. F.; Escudero, M. L. *Surf. Sci.* **1999**, *430*, 206−212.

(41) Bain, C. D. *J. Chem. Soc., Faraday Trans.* **1995**, *91*, 1281−1296.

(42) Nuzzo, R. G.; Dubois, L. H.; Allara, D. L. *J. Am. Chem. Soc.* **1990**, *112*, 558−569.

(43) Wang, Y.; Solano-Canchaya, J. G.; Alcamí, M.; Busnengo, H. F.; Martín, F. *J. Am. Chem. Soc.* **2012**, *134*, 13224−13227.

(44) Widrig, C. A.; Chung, C.; Porter, M. D. *J. Electroanal. Chem.* **1991**, *310*, 335−359.

(45) Fonticelli, M. H.; Benitez, G.; Carro, P.; Azzaroni, O.; Salvarezza, R. C.; Gonzalez, S.; Torres, D.; Illas, F. *J. Phys. Chem. C* **2008**, *112*, 4557−4563.

(46) Corthey, G.; Rubert, A. A.; Benitez, G. A.; Fonticelli, M. H.; Salvarezza, R. C. *J. Phys. Chem. C* **2009**, *113*, 6735−6742.

(47) Yang, D.-F.; Wilde, C. P.; Morin, M. *Langmuir* **1997**, *13*, 243−249.

(48) Azzaroni, O.; Vela, M. E.; Andreasen, G.; Carro, P.; Salvarezza, R. C. *J. Phys. Chem. B* **2002**, *106*, 12267−12273.

(49) Fonticelli, M.; Azzaroni, O.; Benitez, G.; Martins, M. E.; Carro, P.; Salvarezza, R. C. *J. Phys. Chem. B* **2004**, *108*, 1898−1905.

(50) Kakiuchi, T.; Usui, H.; Hobara, D.; Yamamoto, M. *Langmuir* **2002**, *18*, 5231−5238.

(51) Williams, J. A.; Gorman, C. B. *J. Phys. Chem. C* **2007**, *111*, 12804−12810.

(52) Pajkossy, T.; Kolb, D. M. *Electrochim. Acta* **2008**, *53*, 7403−7409.

(53) Drazic, D. M.; Tripkovic, A. V.; Popovic, K. D.; Lovic, J. D. *J. Electroanal. Chem.* **1999**, *466*, 155−164.

(54) Damaskin, B. B.; Petrii, O. A.; Batrakov, V. V. *Adsorption of Organic Compounds on Electrodes*; Plenum Press: New York, 1971.

(55) Lemay, D. M.; Shepherd, J. L. *Electrochim. Acta* **2008**, *54*, 388−393.

(56) Godino, N.; Borrisé, X.; Muñoz, F. X.; Del Campo, F. J.; Compton, R. G. *J. Phys. Chem. C* **2009**, *113*, 11119−11125.

(57) Menshykau, D.; Compton, R. G. *Langmuir* **2009**, *25*, 2519−2529.

(58) Bard, A. J.; Faulkner, L. R. *Electrochemical Methods. Fundamentals and Applications*, 2nd ed.; John Wiley & Sons, Inc.: New York, 2001.

(59) Karhánek, D.; Bučko, T.; Hafner, J. *J. Phys.: Condens. Matter* **2010**, *22*, 265005.

(60) Vericat, C.; Vela, M. E.; Benitez, G.; Carro, P.; Salvarezza, R. C. *Chem. Soc. Rev.* **2010**, *39*, 1805−1834.

(61) Carro, P.; Corthey, G.; Rubert, A. A.; Benitez, G. A.; Fonticelli, M. H.; Salvarezza, R. C. *Langmuir* **2010**, *26*, 14655−14662.

(62) Kautz, N. A.; Kandel, S. A. *J. Am. Chem. Soc.* **2008**, *130*, 6908−6909.

(63) Kautz, N. A.; Kandel, S. A. *J. Phys. Chem. C* **2009**, *113*, 19286−19291.

(64) Grumelli, D.; Vericat, C.; Benitez, G.; Vela, M. E.; Salvarezza, R. C.; Giovanetti, L. J.; Ramallo-López, J. M.; Requejo, F. G.; Craievich, A. F.; Shon, Y. S. *J. Phys. Chem. C* **2007**, *111*, 7179−7184.

(65) Cortés, E.; Rubert, A. A.; Benitez, G.; Carro, P.; Vela, M. E.; Salvarezza, R. C. *Langmuir* **2009**, *25*, 5661−5666.

(66) Mayrhofer, K. J. J.; Blizanac, B. B.; Arenz, M.; Stamenkovic, V. R.; Ross, P. N.; Markovic, N. M. *J. Phys. Chem. B* **2005**, *109*, 14433−14440.

(67) Terán Arce, F.; Vela, M. E.; Salvarezza, R. C.; Arvia, A. J. *Langmuir* **1998**, *14*, 7203−7212.

(68) Orive, A. G.; Grumelli, D.; Vericat, C.; Ramallo-Lopez, J. M.; Giovanetti, L.; Benitez, G.; Azcarate, J. C.; Corthey, G.; Fonticelli, M. H.; Requejo, F. G.; Creus, A. H.; Salvarezza, R. C. *Nanoscale* **2011**, *3*, 1708−1716.

(69) Thomas, J. E.; Humana, R. M.; Real, S. G.; Milocco, R. H.; Castro, E. B. *Int. J. Hydrogen Energy* **2012**, *37*, 10165−10171.

(70) Sheng, W.; Gasteiger, H. A.; Shao-Horn, Y. *J. Electrochem. Soc.* **2010**, *157*, B1529−B1536.

(71) Humana, R. M.; Thomas, J. E.; Ruiz, F.; Real, S. G.; Castro, E. B.; Visintin, A. *Int. J. Hydrogen Energy* **2012**, *37*, 14966−14971.

(72) Visintin, A.; Castro, E. B.; Real, S. G.; Triaca, W. E.; Wang, C.; Soriaga, M. P. *Electrochim. Acta* **2006**, *51*, 3658−3667.

(73) Thomas, J. E.; Castro, E. B.; Visintin, A. *Int. J. Hydrogen Energy* **2010**, *35*, 5981−5984.

(74) Borodziński, A.; Bonarowska, M. *Langmuir* **1997**, *13*, 5613−5620.

(75) Lopez-Sanchez, J. A.; Dimitratos, N.; Hammond, C.; Brett, G. L.; Kesavan, L.; White, S.; Miedziak, P.; Tiruvalam, R.; Jenkins, R. L.; Carley, A. F.; Knight, D.; Kiely, C. J.; Hutchings, G. J. *Nat. Chem.* **2011**, *3*, 551−556.